Journal of the Korean Magnetic Resonance Society **2014**, *18*, 15-23
DOI 10.6564/JKMRS.2014.18.1.015

Nucleus–phonon interactions of $MCsSO_4$ (M = Na, K, or Rb) single crystals studied using spin–lattice relaxation time

Jae Hun Choi[1], Nam Hee Kim[1], and Ae Ran Lim[1, 2,*]

[1] Department of Carbon Fusion Engineering, Jeonju University, Jeonju 560-759, Korea
[2] Department of Science Education, Jeonju University, Jeonju 560-759, Korea

Received April 10, 2014; Revised May 2, 2014; Accepted June 10, 2014

Abstract The structural properties and relaxation processes of $MCsSO_4$ (M = Na, K, or Rb) crystals were investigated by measuring the NMR spectra and spin–lattice relaxation rates $1/T_1$ of their ^{23}Na, ^{39}K, ^{87}Rb, and ^{133}Cs nuclei. According to the NMR spectra, the $MCsSO_4$ crystals contain two crystallographically inequivalent sites each for the M and Cs ions. Further, the relaxation rates of all these nuclei do not change significantly over the investigated temperature range, indicating that no phase transitions occur in these crystals in this range. The variations in the $1/T_1$ values of the ^{23}Na, ^{39}K, ^{87}Rb, and ^{133}Cs nuclei in these three crystals with increasing temperature are approximately proportional to T^2, indicating that Raman processes may be responsible for the relaxation. Therefore, for nuclear quadrupole relaxation of the ^{23}Na, ^{39}K, ^{87}Rb, and ^{133}Cs nuclei, Raman processes with n = 2 are more effective than direct processes.

Keywords: $NaCsSO_4$, $KCsSO_4$, $RbCsSO_4$, Nuclear magnetic resonance, Raman process, Relaxation time.

Introduction

Double sulfate crystals are members of a family of crystals with the general formula $MM'BX_4$, where M and M' represent the monovalent ions Li^+, Na^+, K^+, Rb^+, or Cs^+, and BX_4 denotes SO_4^{2-} or SeO_4^{2-} [1-8]. For example, sodium cesium sulfate, $NaCsSO_4$, potassium cesium sulfate, $KCsSO_4$, and rubidium cesium sulfate, $RbCsSO_4$, are double sulfate crystals. The physical properties and phase transitions of double sulfate crystals have attracted considerable interest because of their anomalous behaviors at their transition temperatures [9-13] and their interesting structural phase transition sequences [14-17], in particular those between their ferroelectric, ferroelastic, and superionic phases. The properties of these phases are currently of great interest because of possible applications of these crystals in energy sources [18, 19]. $MCsSO_4$ (M = Na, K, or Rb) crystals also have potential applications, but no research into their physical properties or NMR relaxation processes has been reported.

The spin–lattice relaxation rates of a crystal can be used as measures of its dynamics and indicate the ease with which the excited-state energies of the crystal nuclear systems are transferred to its lattice. In this study, detailed information about the relaxation mechanisms of $MCsSO_4$ (M = Na, K, or Rb) crystals was obtained by measuring the spin–lattice relaxation rates $1/T_1$ of their constituent

* Address correspondence to: **Ae Ran Lim,** Tel:+82-(0)63-220-2514; Fax: +82-(0)63-220-2053; E-mail: aeranlim@hanmail.net, arlim@jj.ac.kr

nuclei, ^{23}Na, ^{39}K, ^{87}Rb, and ^{133}Cs. We determined the temperature dependences of $1/T_1$ for these nuclei for the first time by using pulse NMR spectrometry. The NMR results were used to determine the relaxation mechanisms for these three crystals and to characterize their Raman processes. This paper also reports the effect of nucleus–phonon interactions on the ^{23}Na, ^{39}K, ^{87}Rb, and ^{133}Cs nuclei in the three crystals.

Experimental section

Single $MCsSO_4$ crystals (M = Na, K, or Rb) were grown from aqueous solutions containing Na_2SO_4:Cs_2SO_4, K_2SO_4:Cs_2SO_4, and Rb_2SO_4:Cs_2SO_4, respectively, by using the slow evaporation method at 293 K. The resulting crystals had hexagonal shapes and were colorless and transparent.

Differential scanning calorimetry (DSC) was performed on the three crystals using a DuPont 2010 DSC instrument in order to determine their phase transition temperatures. These measurements were performed at a heating rate of 10 K/min. No phase transitions were found for the three crystals between 120 and 530 K.

The NMR signals of the ^{23}Na, ^{39}K, ^{87}Rb, and ^{133}Cs nuclei in the $MCsSO_4$ (M = Na, K, or Rb) single crystals were measured using a Bruker 400 FT NMR spectrometer at the Korea Basic Science Institute. The static magnetic field was 9.4 T, and the central radio frequencies were $\omega_o/2\pi$ = 105.84 MHz for the ^{23}Na nuclei, 18.67 MHz for the ^{39}K nuclei, 130.93 MHz for the ^{87}Rb nuclei, and 52.48 MHz for the ^{133}Cs nuclei. For the T_1 measurements, $\pi/2$–t–$\pi/2$ pulse sequences were used with the saturation recovery method. The nuclear magnetizations $S(t)$ of the ^{23}Na, ^{39}K, ^{87}Rb, and ^{133}Cs nuclei at time t after the $\pi/2$ pulses were determined from the saturation recovery sequences. The widths of the $\pi/2$ pulses were 0.5 μs for ^{23}Na, 20 μs for ^{39}K, and 1.65 μs for ^{87}Rb. Further, the widths for ^{133}Cs in the three crystals ranged from 5 to 17 μs. Temperature-dependent NMR measurements were obtained over the temperature range 180–420 K; NMR data could not be obtained above 420 K because the NMR spectrometer did not have adequate temperature control at high temperatures. The samples were maintained at a constant temperature (accuracy ±0.5°C) by controlling the nitrogen gas flow and heater current.

Experimental results and analysis

1. Theoretical background

We describe the recovery laws for the quadrupole relaxation processes in the ^{23}Na (I = 3/2), ^{39}K (I = 3/2), and ^{87}Rb (I = 3/2) nuclear spin systems. The transition probabilities for $\Delta m = \pm 1$ and $\Delta m = \pm 2$ are denoted by W_1 and W_2, respectively. The rate equations can then be expressed as [20]

$$\begin{aligned} dn_{-3/2}/dt &= -(W_1 + W_2)n_{-3/2} + W_1 n_{-1/2} + W_2 n_{1/2} \\ dn_{-1/2}/dt &= -W_1 n_{-3/2} + (W_1 + W_2)n_{-1/2} + W_2 n_{3/2} \\ dn_{1/2}/dt &= W_2 n_{-3/2} - (W_1 + W_2)n_{1/2} + W_1 n_{3/2} \\ dn_{3/2}/dt &= W_2 n_{-1/2} + W_1 n_{1/2} - (W_1 + W_2)n_{3/2} \end{aligned} \quad (1)$$

where $n_{-3/2}$, $n_{-1/2}$, $n_{1/2}$, and $n_{3/2}$ are the differences in population between the equilibrium value and that at time t for each energy level. The eigenvalues of these equations are W_1, W_2, and $W_1 + W_2$.

The saturation recovery traces for the central line of ^{23}Na, ^{39}K, and ^{87}Rb with dominant quadrupole relaxation in $MCsSO_4$ (M = Na, K, or Rb) crystals can be represented by a combination of two exponential functions [20, 21]:

$$S(t) = S(\infty)\{1 - 0.5[\exp(-2W_1 t) + \exp(-2W_2 t)]\} \quad (2)$$

here $S(t)$ is the nuclear magnetization corresponding to the central transition at time t after saturation. The spin–lattice relaxation rate is given by [22]

$$1/T_1 = 0.4(W_1 + 4W_2) \quad (3)$$

When only the central line is excited, the magnetization recovery of the ^{133}Cs nuclei in the $MCsSO_4$ (M = Na, K, or Rb) crystals does not follow a single exponential function but can be represented by a combination of four exponential functions. The signal for $W_1 = W_2$ is given by [23-25]

$$[S(\infty) - S(t)] / S(\infty) = 0.048 \exp(-0.476W_1t) + 0.818 \exp(-1.333W_1t) + 0.050 \exp(-2.381W_1t) + 0.084 \exp(-3.810W_1t) \quad (4)$$

where $S(t)$ is the nuclear magnetization corresponding to the central transition at time t, and W_1 and W_2 are the transition probabilities corresponding to $\Delta m = \pm 1$ and $\Delta m = \pm 2$, respectively. The return to equilibrium is characterized by four relaxation times.

The interaction of the nuclear quadrupole moment with the lattice vibrations is a very important relaxation mechanism for nuclear spin $I \geq 1$ in many crystals. The coupling can generally be represented in terms of a spin–lattice Hamiltonian [26],

$$\mathcal{H} = \sum_q F^{(q)} A^{(q)} \quad (5)$$

where $F^{(q)}$ and $A^{(q)}$ are the lattice and spin operators of order q, respectively. $F^{(q)}$ (hereafter, we omit the index q for brevity) can be defined as a function of the stress tensor σ:

$$F = F_o + F_1\sigma + F_2\sigma^2 + F_3\sigma^3 + \ldots \quad (6)$$

At temperatures far below the melting temperature of the crystal, the thermal stress is expected to be small, so only the first few terms in Eq. (6) are important. The term $F_1\sigma$ represents the absorption or emission of a single phonon (the direct process), and the next term, $F_2\sigma^2$, corresponds to the emission or absorption of two phonons or the absorption of one phonon followed by the emission of another one (Raman processes). In the direct process, the spin–lattice relaxation rate $1/T_1$ is proportional to the square of the frequency ω_o and to the absolute temperature. At low temperatures, the direct process might be effective, but it is nearly negligible for the spin–lattice relaxation of nuclear spins with nuclear quadrupole moments. At the high-temperature limit, on the other hand, the Raman processes yield a relaxation rate that is proportional to the square of the temperature. Note that the direct and Raman processes are both first-order processes within perturbation theory with perturbing Hamiltonians $F_1\sigma$ and $F_2\sigma^2$, respectively. It has also been suggested that a second-order contribution to the relaxation rate might arise from interference between the spin–lattice term $F_1\sigma$ and the inharmonic term $F_3\sigma^3$ in the lattice energy, which is responsible for the thermal conductivity. The contributions of the interference between terms of higher order to either the spin–lattice coupling $F_m\sigma^m$ or the lattice energy $G_m\sigma^m$ are small.

2. ^{23}Na and ^{133}Cs NMR in a $NaCsSO_4$ single crystal

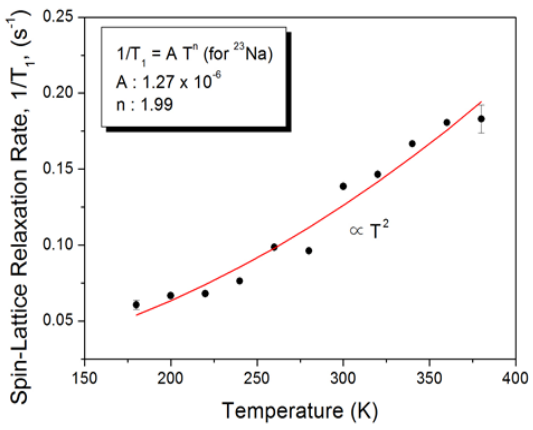

Figure 1. Temperature dependence of $1/T_1$ for ^{23}Na in a $NaCsSO_4$ single crystal. Solid curve is described by $1/T_1 = AT^n$

The ^{23}Na (I=3/2) NMR spectrum of $NaCsSO_4$ crystals consists of a central line and two satellite lines. When the magnetic field was applied along the crystal's c-axis, the resonance lines of ^{23}Na were observed. The ^{23}Na spectrum of a $NaCsSO_4$ single crystal was recorded at several temperatures. The spectral features suggest the presence of two types of crystallographically inequivalent ^{23}Na nuclei, Na(1) and Na(2). The nuclear magnetization recovery curves of the ^{23}Na nuclei were obtained by measuring the nuclear magnetization after applying saturation pulses. The recovery traces for the central resonance line of ^{23}Na with dominant quadrupole relaxation can be represented by a combination of the two exponential functions in Eq. (2). The temperature dependences of the ^{23}Na spin–lattice transition rates W_1 and W_2 were obtained from Eq. (2): W_1 and W_2 both increase with increasing temperature. W_1 is

nearly equal to W_2 up to approximately 400 K. If W_1 and W_2 have the same values in the recovery traces of ^{23}Na in $NaCsSO_4$ crystals, we can discuss the relaxation rate according to $1/T_1 = 2W_1$ [see Eq. (2)]. When $W_1 \neq W_2$, the constant $0.4(W_1 + 4W_2)$ is introduced instead of $1/T_1$; this constant is identical to $1/T_1$ when $W_1 = W_2$. The temperature dependence of $1/T_1$ for the ^{23}Na nuclei is shown in Fig. 1 The value of $1/T_1$ increases slowly with increasing temperature. The relaxation rates of the ^{23}Na nuclei do not change significantly in the investigated temperature range, which indicates that no phase transitions occur at these temperatures.

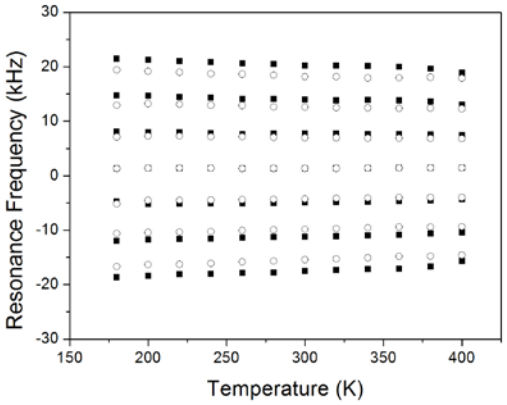

Figure 2. Separation of the ^{133}Cs resonance lines in a $NaCsSO_4$ single crystal as a function of temperature.

The seven-line structure of the ^{133}Cs (I=7/2) NMR spectrum is the result of the quadrupole interaction. When the crystal is rotated about its crystallographic axis, crystallographically equivalent nuclei produce seven lines, that is, one central line and six satellite lines. However, two groups of resonance lines were observed in the ^{133}Cs NMR spectrum for the $NaCsSO_4$ single crystal, as shown in Fig. 2; the zero point of the y axis corresponds to the resonance frequency $\omega_o/2\pi$ = 52.48 MHz of the ^{133}Cs nucleus. This result indicates the presence of two types of crystallographically inequivalent ^{133}Cs nuclei, Cs(1) and Cs(2). The satellite transitions are well resolved from the central line, and the signal intensity of the central line is stronger than those of the other lines. The central transition is virtually unshifted by the quadrupole interaction, and the separations between the lines varies with temperature (see Fig. 2). The splitting between the resonance lines decreased slowly with increasing temperature for the two types of Cs resonance lines; thus, the quadrupole coupling constants of the two groups decreased with increasing temperature, indicating that the two types of ^{133}Cs nuclei have different quadrupole parameters. The variation in the splitting of the ^{133}Cs resonance lines with temperature indicates a change in the electric field gradient (EFG) at the Cs sites, which in turn indicates that the atoms neighboring the ^{133}Cs nuclei are displaced as the temperature changes.

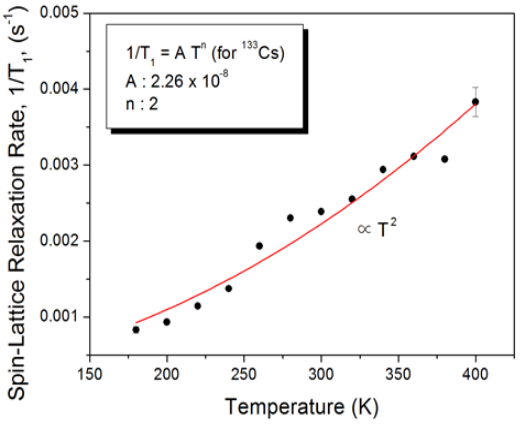

Figure 3. Temperature dependence of $1/T_1$ for ^{133}Cs in a $NaCsSO_4$ single crystal. Solid curve is described by $1/T_1 = AT^n$.

The nuclear magnetization recovery traces for ^{133}Cs were measured at several temperatures; those for the central resonance line of ^{133}Cs with dominant quadrupole relaxation can be represented by a combination of four exponential functions, as in Eq. (4). The slope of each trace increases with increasing temperature. We measured the variation with temperature of the spin–relaxation rate $1/T_1$ for the central resonance line of the Cs nuclei. We obtained $1/T_1$ for ^{133}Cs in terms of W_1 and W_2 using Eq. (4); it increased slowly with increasing temperature, as shown in Fig. 3. The central resonance lines Cs(1) and Cs(2) overlap, so the relaxation rates of these nuclei cannot be distinguished. The relaxation rates of the ^{133}Cs nuclei do not change significantly in this temperature range.

According to our experimental results, the temperature dependences of $1/T_1$ for $NaCsSO_4$ can be

described by the approximations $1/T_1 = (1.27 \times 10^{-6})T^{1.99}$ for the Na nuclei and $1/T_1 = (2.26 \times 10^{-8})T^2$ for the Cs nuclei, which are shown as solid curves in Figs. 1 and 3, respectively.

3. ^{39}K and ^{133}Cs NMR in a $KCsSO_4$ single crystal

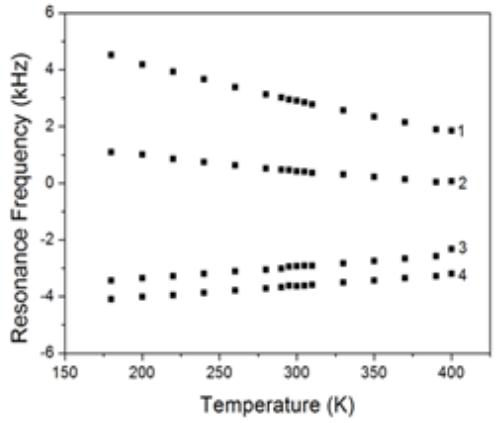

Figure 4. Separation of the ^{39}K resonance lines in a $KCsSO_4$ single crystal as a function of temperature.

The ^{39}K (I = 3/2) NMR spectrum usually consists of a central line and a pair of satellite lines. When the crystal is rotated about the crystallographic axis, crystallographically equivalent ^{39}K nuclei produce three lines: one central line and two satellite lines. The magnitudes of the quadrupole parameters of ^{39}K nuclei are on the order of MHz, so usually only the central line is obtained. The satellite lines are located far from the central line and so are difficult to obtain. However, four resonance lines were obtained for the ^{39}K nuclei in $KCsSO_4$ crystals. They indicate the presence of two types of crystallographically inequivalent ^{39}K nuclei and two types of magnetically inequivalent ^{39}K nuclei. The variations with temperature in the ^{39}K spectra are shown in Fig. 4. The zero point of the y axis corresponds to the resonance frequency of the ^{39}K nucleus (18.67 MHz). The ^{39}K resonance frequency of $KCsSO_4$ decreases with increasing temperature, and the resonance line shifts are strongly temperature dependent. The changes in the splitting of the ^{39}K resonance line cause the EFG at the ^{39}K sites to vary as the atoms neighboring ^{39}K are displaced from their room temperature positions.

The variation as a function of delay time in the nuclear magnetization for 39K was measured at several temperatures; the saturation recovery traces can be represented by a combination of the two exponential functions in Eq. (2). Here, the slopes of

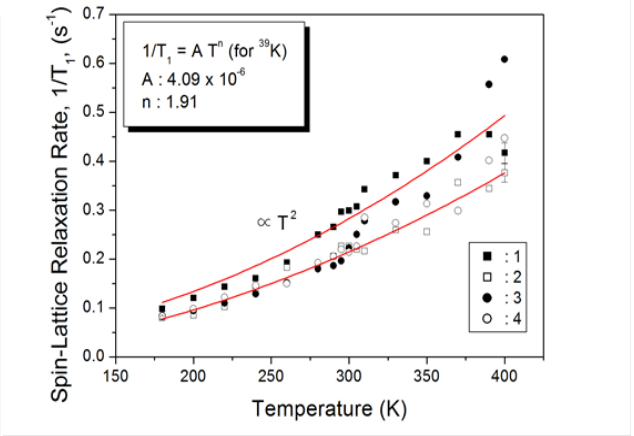

Figure 5. Temperature dependence of 1/T1 for 39K in a KCsSO4 single crystal. Solid curve is described by $1/T_1 = AT^n$.

the plots of ln [S(∞) – S(t)]/S(∞) vs. t are nonlinear because the traces are combinations of two exponential functions.

The relaxation rates W_1 and W_2 for the ^{39}K resonance line were measured at a frequency of $\omega_o/2\pi$ = 18.67 MHz as a function of temperature. The values of W_1 and W_2 obtained from Eq. (2) exhibited similar temperature dependences, and the relaxation rate obtained from the W_1 and W_2 values was $0.4(W_1 + 4W_2)$. Figure 5 shows the temperature dependences of the ^{39}K nuclear spin–lattice relaxation rate for the four central resonance lines, which are very similar; as the temperature increases, $1/T_1$ increases slowly.

We also obtained the ^{133}Cs (I = 7/2) NMR spectrum for a single $KCsSO_4$ crystal at room temperature. Two groups of resonance lines, each consisting of a strong central line and six well-resolved satellite lines, were observed when the magnetic field was applied along the c-axis. These spectral features indicate the presence of two types of crystallographically inequivalent ^{133}Cs nuclei, Cs(1) and Cs(2). The central transition remains almost unshifted by the quadrupole interaction between 180 and 400 K, and the resonance line splitting between the satellite lines

varies with temperature. The spin–lattice relaxation rates of ^{133}Cs in $KCsSO_4$ were measured, and the recovery traces of the magnetization were determined for this crystal at several temperatures. In dominant quadrupole relaxation, such as for $KCsSO_4$, the recovery trace of the central resonance line of ^{133}Cs can be represented by a combination of four exponential functions, as in Eq. (4). We determined the variation with temperature in the relaxation rate for the central resonance line of the ^{133}Cs nuclei. This spin–lattice relaxation rate $1/T_1$ was obtained by using the saturation method; it was determined in terms of W_1 using Eq. (4). The temperature dependence of $1/T_1$ is shown in Fig. 6. The trend for the temperature dependence of $1/T_1$ for the ^{133}Cs nuclei differs from that for the ^{39}K nuclei in this temperature range.

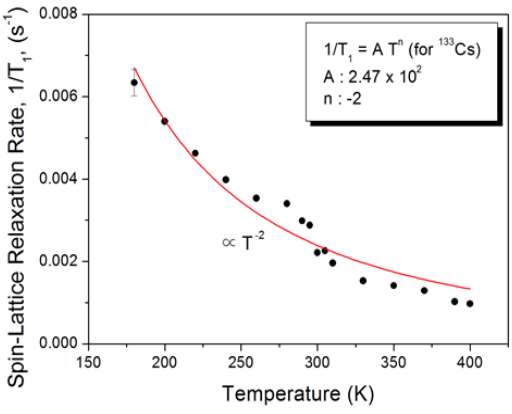

Figure 6. Temperature dependence of $1/T_1$ for ^{133}Cs in a $KCsSO_4$ single crystal. Solid curve is described by $1/T_1 = AT^n$.

The NMR results revealed that the temperature dependences of $1/T_1$ for $KCsSO_4$ can be represented by the approximations $1/T_1 = (4.09 \times 10^{-6})T^{1.91}$ for the K nuclei and $1/T_1 = (2.47 \times 10^{2})T^{-2}$ for the Cs nuclei, which are shown as solid curves in Figs. 5 and 6, respectively. These relationships are consistent with Raman processes, which depend on T^2.

4. ^{87}Rb and ^{133}Cs NMR in a $RbCsSO_4$ single crystal

Figure 7 shows the ^{87}Rb (I = 3/2) NMR spectrum of crystalline $RbCsSO_4$, which was obtained at a frequency of $\omega_o/2\pi$ = 130.88 MHz with the magnetic field applied along the c-axis. When a crystal with crystallographically equivalent nuclei is rotated about the crystallographic axis, the nuclei produce three lines, one central line and two satellite lines. Here, instead of one central resonance line for the ^{87}Rb nuclei, four central resonance lines were obtained. The reason is that two types of crystallographically inequivalent Rb nuclei, Rb(1) and Rb(2), and two types of magnetically inequivalent Rb nuclei, were present. The four resonance lines correspond to the central transitions ($+1/2 \leftrightarrow -1/2$). Signals 1, 2, 3, and 4 for the ^{87}Rb nuclei are assigned in Fig. 7. Although lines 2 and 3 appear to be constant, lines 1 and 4 change slightly in position as the temperature changes, as shown in Fig. 7. These changes indicate that the EFG at the ^{87}Rb sites varies with temperature, suggesting that the atoms neighboring ^{87}Rb are displaced.

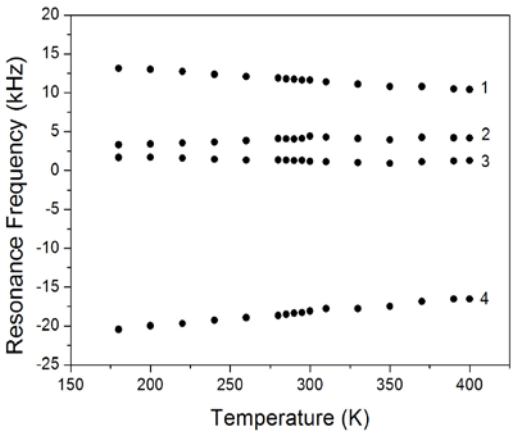

Figure 7. Separation of the ^{87}Rb resonance lines in a $RbCsSO_4$ single crystal as a function of temperature.

The $1/T_1$ values for the four central resonance lines of ^{87}Rb were determined as functions of temperature. The saturation recovery curves were measured at several temperatures, and the recovery traces for these lines with dominant quadrupole relaxation can be expressed as combinations of two exponential functions, as in Eq. (2). Consequently, the slopes of the plots of ln $\{[S(\infty) - S(t)]/S(\infty)\}$ vs. t are nonlinear. The relaxation rates W_1 and W_2 of ^{87}Rb in $RbCsSO_4$ exhibit similar trends with increasing temperature, and W_1 is less than W_2 at all temperatures. The relaxation rate obtained from the W_1 and W_2 values

was $0.4(W_1 + 4W_2)$. The temperature dependences of $1/T_1$ for the ^{87}Rb nuclei in this single crystal are shown in Fig. 8, where the symbols ■, □, ●, and ○ denote $1/T_1$ for signals 1, 2, 3, and 4, respectively.

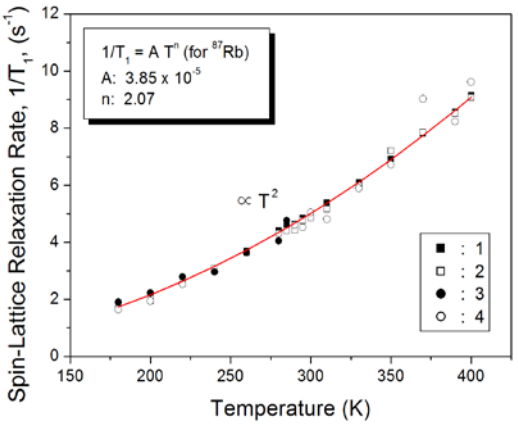

Figure 8. Temperature dependence of 1/T1 for 87Rb in a RbCsSO4 single crystal. Solid curve is described by 1/T1=ATn.

The $1/T_1$ values for the four signals agree within the experimental error.

The NMR spectrum of ^{133}Cs (I = 7/2) was obtained at several temperatures. Seven resonance lines were observed when the magnetic field was applied along the crystallographic c axis. The ^{133}Cs NMR spectrum of $RbCsSO_4$ single crystals contains fourteen lines in two groups. The two groups of resonance lines for the Cs nuclei are caused by crystallographically inequivalent sites, Cs(1) and Cs(2). The central transition is almost unshifted by the quadrupole interaction, and the splitting between the satellite lines varies with temperature. This variation indicates that the EFG at the Cs sites, and thus the displacements of the atoms neighboring ^{133}Cs, vary with temperature. The recovery trace for the central line of ^{133}Cs in $RbCsSO_4$ crystals can be represented by a combination of four exponential functions. The ^{133}Cs relaxation time was obtained in terms of W_1 ($T_1 = 1/1.333W_1$), and the temperature dependence of the ^{133}Cs spin–lattice relaxation rate $1/T_1$ is shown in Fig. 9.

The temperature dependences of $1/T_1$ for ^{87}Rb and ^{133}Cs in $RbCsSO_4$ can be described by the approximations $1/T_1 = (3.85 \times 10^{-5})T^{2.07}$ and $1/T_1 = (1.06 \times 10^{1})T^{-2}$, respectively. These approximations are consistent with Raman processes, which depend on T^2.

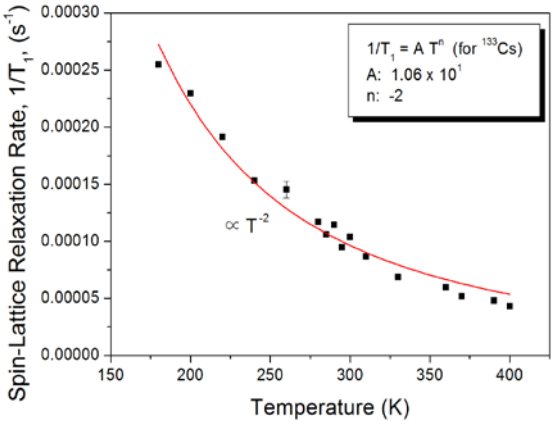

Figure 9. Temperature dependence of $1/T_1$ for ^{133}Cs in a $RbCsSO_4$ single crystal. Solid curve is described by $1/T_1 = AT^n$.

Discussion and conclusions

The structural properties and relaxation processes in $MCsSO_4$ (M = Na, K, or Rb) crystals were investigated by determining their NMR spectra and the spin–lattice relaxation rates of their ^{23}Na, ^{39}K, ^{87}Rb, and ^{133}Cs nuclei. The NMR spectra show that the $MCsSO_4$ crystals contain two crystallographically inequivalent types each for the M and Cs ions. These results are consistent with previously reported results for the K and Na nuclei in $KNaSO_4$ crystals [27]. Further, the variations in the $1/T_1$ values of ^{23}Na, ^{39}K, and ^{87}Rb in the three crystals with increasing temperature are approximately proportional to T^2. However, at a given temperature, $1/T_1$ for the ^{133}Cs nuclei in $KCsSO_4$ and $RbCsSO_4$ differs from that for the ^{133}Cs nuclei in $NaCsSO_4$; the values are inversely proportional to the square of the temperature, T^{-2}, in $KCsSO_4$ and $RbCsSO_4$, whereas the value is proportional to the square of the temperature, T^2, in $NaCsSO_4$. These results suggest that differences between the ^{133}Cs nuclei due to their distinct local environments are responsible for these differences in the $1/T_1$ values of ^{133}Cs. The ionic radii of Na, K, and Rb ions are 0.97, 1.33, and 1.47 Å, respectively.

Further, the electronegativity of Na ions is 0.93, and that of both Rb and K is 0.82. Consequently, when Rb ions replace K ions, the EFG at the resonant nucleus is determined by an identical ionic contribution around the resonant nucleus. There are two contributions to the EFG: the internal atomic contribution due to the electrons surrounding the nuclei and the external ionic contribution due to the neighboring ions [28]. According to our experimental results, the Cs NMR $1/T_1$ is very much shorter than those of Na, K, and Rb. The differences between the $1/T_1$ values of the four nuclei can be attributed to their different Larmor and quadrupole frequencies, among other factors. These differences arise from differences in the electric quadrupole moments of Na, K, Rb, and Cs (Q_{Na}: 10.4×10^{-30} m^2, Q_K: 5.85×10^{-30} m^2, Q_{Rb}: 13.35×10^{-30} m^2, and Q_{Cs}: -0.343×10^{-30} m^2); $1/T_1$ is proportional to the square of the quadrupole coupling constant [$1/T_1 \propto (e^2qQ/h)^2$] [29, 30].

The relaxation rates for the ^{23}Na, ^{39}K, ^{87}Rb, and ^{133}Cs nuclei in the three crystals can be described by $1/T_1 \propto AT^2$, which is consistent with Raman processes. The dominant relaxation mechanism for nuclei possessing electric quadrupole moments is provided by the coupling of these moments to the thermal fluctuations of the local EFGs via Raman spin–phonon processes. A theory of nuclear quadrupolar spin–lattice relaxation was first proposed by Van Kranendonk [31, 32]. According to Van Kranendonk [33], the contribution of a Raman process to the spin–lattice relaxation rate is given by $1/T_1 = (T^*)^2 f(T^*)$, where the reduced temperature $T^* = T/\Theta$ (Θ is the Debye temperature). The function $f(T^*)$ is proportional to $(T^*)^5$ in the low-temperature limit, $T^* << 0.02$. In contrast, $f(T^*)$ is constant in the high-temperature limit, $T^* > 0.5$ [33]. Thus, in all of the cases considered, Raman processes that depend on T^2 are more effective for nuclear quadrupole relaxation than direct processes. The $1/T_1$ results for ^{23}Na, ^{39}K, ^{87}Rb, and ^{133}Cs in the three crystals can be explained in terms of a relaxation mechanism in which the lattice vibrations are coupled to the nuclear electric quadrupole moments, as described above.

Acknowledgement

This research was supported by the Basic Science Research program through the National Research Foundation of Korea (NRF) funded by the Ministry of Education, Science, and Technology (2012001763).

References

1. H.I. Abd El-Kader, Qatar Univ. Sci. J. **14**(c), 100 (1994).
2. S.M. Haile, D.A. Boysen, C.R.I. Chisholm, R.B. Merle, Nature **410**, 910 (2001).
3. H. Kamimura, S. Watanabe, Philos. Mag. B**81**, 1011 (2001).
4. Y. Matsuo, K. Takahashi, S. Ikehata, J. Phys. Soc. Jpn. **70**, 2934 (2001).
5. T. Norby, Nature **410**, 877 (2001)
6. Y. Matsuo, K. Takahashi, S. Ikehata, Solid State Commun. **120**, 85 (2001).
7. Y. Matsuo, K. Takahashi, S. Ikehata, Ferroelectrics **272**, 199 (2002).
8. H. Kamimura, Y. Matsuo, S. Ikehata, T. Ito, M. Komukae, T. Osaka, Phys. Status Solidi B **241**, 61 (2004).
9. B. Mroz, T. Krajewsk, T. Breczewski, W. Chomka, D. Semotowicz, Ferroelectrics **42**, 459 (1982).
10. T. Krajewski, T. Breczewski, M. Kassem, B. Mroz, Ferroelectrics **55**, 811 (1984).
11. M.E. Kassem, S.H. Kandil, E.F. El-Wahidy, M. El-Gamal, Rev. Phys. Appl. **19**, 445 (1984).
12. M.E. Kassem, S. Hedewy, J. Mat. Sci. Lett. **7**, 1007 (1988).
13. K.S. Aleksandrov, I.L. Zherebtsova, I.M. Iskornev, A.I. Kruglik, O.V. Rozanor, I.N. Flerov, Sov. Phys.

Solid State **22**, 215 (1980).
14. H. Mashiyama, K. Hasebe, S. Tanisaki, Y. Shiroishi, S. Sawada, J. Phys. Soc. Japan **47**, 1198 (1979).
15. B. Kihal, C. Dugautier, R. Farhi, P. Moch, J. Phys. C **20**, 4491 (1987).
16. T. Mitsui, T. Oka, Y. Shiroishi, M. Takashige, K. Lio, S. Swada, J. Phys. Soc. Japan **39**, 845 (1975)
17. M.E. Hiues, A.M. Glass, Principles and Applications of Ferroelectrics and Related Materials. Clarendon Press, Oxford.
18. M.E. Kassem, A.M. El-Katib, E.F. El-Wahidy, H.E. Gado, J. Mat. Sci. Lett. **6**, 507 (1987).
19. H.P. Beerman, Ferroelectrics **2**, 123 (1977).
20. M. Igarashi, H. Kitagawa, S. Takahashi, R. Yoshizak, Y. Abe, Z. Naturforsch. **47a**, 313 (1992).
21. J.J. Van der Klink, D. Rytz, F. Borsa, U.T. Hochi, Phys. Rev. B **27**, 89 (1983).
22. A. Avogadro, E. Cavelius, D. Muller, J. Petersson, Phys. Status Solidi B **44**, 639 (1971).
23. E.R. Andrew, D.P. Tunstall, Proc. Phys. Soc. (London) **78**, 1 (1961).
24. D.P. Tewari, G.S. Verma, Phys. Rev. **129**, 1975 (1963).
25. M.A. Gordon, M.J.R. Hoch, J. Phys. C: Solid State Phys. **11**, 783 (1978).
26. A, Abragam, The Principles of Nuclear Magnetism, Oxford University Press, Oxford (1961).
27. A.R. Lim, I.H. Choi, J.-H. Chang, Phys. Status Solidi B **246**, 2372 (2009).
28. H.J. Kim, D.Y. Jeong, B. Zalar, R. Blinc, S.H. Choh, Phys. Rev. B **61**, 9307 (2000).
29. R. Bohmer, K.R. Jeffrey, M. Vogel, Prog. Nucl. Magn. Reson. Spectrosc. **50**, 87 (2007).
30. A.R. Lim, J. Appl. Phys. **106**, 93522 (2009).
31. J. Van Kranendonk, M.B. Walker, Phys. Rev. Lett. **18**, 701 (1967).
32. J. Van Kranendonk, Physica B **20**, 781 (1954).
33. J. Van Kranendonk, Can. J. Phys. **46**, 2441 (1968).